Eur. Phys. J. B **48**, 81–86 (2005)
DOI: 10.1140/epjb/e2005-00369-x

THE EUROPEAN PHYSICAL JOURNAL B

Propagation of fronts in activator-inhibitor systems with a cutoff

E.P. Zemskov[1] and V. Méndez[2,a]

[1] Grup de Física Estadística, Departament de Física, Universitat Autònoma de Barcelona, 08193 Bellaterra, Barcelona, Spain
[2] Departament de Medicina, Universitat Internacional de Catalunya, 08190 Sant Cugat del Vallès, Barcelona, Spain

Received 27 April 2005 / Received in final form 25 August 2005
Published online 9 December 2005 –

Abstract. We consider a two-component system of reaction-diffusion equations with a small cutoff in the reaction term. A semi-analytical solution of fronts and how the front velocities vary with the parameters are given for the case when the system has a piecewise linear nonlinearity. We find the existence of a nonequilibrium Ising-Bloch bifurcation for the front speed when the cutoff is present. Numerical results of solutions to these equations are also presented and they allow us to consider the collision between fronts, and the existence of different types of traveling waves emerging from random initial conditions.

PACS. 05.70.Ln Nonequilibrium and irreversible thermodynamics – 05.40.Fb Random walks and Levy flights

The study of front propagation is one of the most fundamental problems in nonequilibrium physics [1]. The concept of cutoff [2–4] has been introduced to model the effects of the discrete nature of the interaction in systems with continuum variables around the unstable state. If one thinks of the continuous system as an approximation to a contact process among N individuals, the cutoff is $1/N$. As the number of particles is an integer, the concentration $u(x,t)$ could be thought of as being larger than some threshold $\varepsilon = 1/N$, which would correspond to the value of $u(x,t)$ when a single particle is present. Most studies [3–5] are concentrated on one-component systems. It was shown that the effect of the cutoff ε is to select a single velocity that converges when $\varepsilon \to 0$ to that predicted by the marginal stability argument [3,4]. This question is, however, still open for two-species systems where the effect of the cutoff may be presumably very important in the existence and the propagation of the fronts. The two-component reactions yield a variety of pattern formations in non-equilibrium systems [6]. In the context of the two-component model with cutoff it was found that for a given diffusion ratio D for both species, there is a critical value $\varepsilon_{\rm crit}$ of the cutoff threshold such that the front is unstable for all $\varepsilon > \varepsilon_{\rm crit}$ [7]. The front is diffusively unstable, as it supports large cellular structures with grooves where growth is screened out [7]. This phenomenon was found by simulations of the simple two-component model

$$\frac{\partial u}{\partial t} = \Delta u + uv,$$
$$\frac{\partial v}{\partial t} = D\Delta v - uv.$$

In this work we will study the dependence of the front velocity on the imposition of a cutoff around a stable state in a two-component reaction-diffusion system with a bistable kinetics or reaction term. This kind of model has been used to simulate the patterns formation of bacterial colonies [8]. We will perform time-dependent numerical simulations to show how uniformly translating front solutions appear from initial conditions with compact support. In order to be able to construct the front solutions semi-analytically, we take the reaction terms piecewise linear. This approach is well known in studies of excitable media [9]. The introduction of the cutoff in the model is represented by equations with reaction functions multiplied by the Heaviside step-function $\theta(u-\varepsilon)$, where $\varepsilon = \text{const}$ is the threshold density for growth (cutoff size) [8]. Thus, the system being considered consists of two scalar fields, an activator $u(x,t)$ and an inhibitor $v(x,t)$, and is described by the equations

$$\frac{\partial u(x,t)}{\partial t} = f(u,v)\theta(u-\varepsilon) + \frac{\partial^2 u(x,t)}{\partial x^2},$$
$$\frac{\partial v(x,t)}{\partial t} = \eta g(u,v)\theta(u-\varepsilon) + \frac{\partial^2 v(x,t)}{\partial x^2} \qquad (1)$$

with reaction terms $f(u,v) = -u + \theta(u-a) - v$ and $g(u,v) = u - v$. Here $\theta(u)$ is the Heaviside function; η is the time scale ratio and a is the position of the discontinuity in $f(u,v)$. This is one of the simplest one-dimensional bistable reaction-diffusion systems involving one activator and one inhibitor. This model was originally presented (with nondiffusing inhibitor $v(x,t)$ and without cutoff) as

[a] e-mail: vmendez@csc.unica.edu

a mathematical description of the excitation and propagation of nerve impulses [10]. In equation (1) we have considered that both activator and inhibitor have the same diffusion coefficient. This assumption simplifies our calculations and is also common for activator-inhibitor systems described by the Belousov-Zhabotinsky reaction [11].

Introducing the traveling frame coordinate $\xi = x - ct$, where c is the wave speed, we obtain two ordinary differential equations. There are two front solutions in the two-component reaction-diffusion systems [12]. For the symmetric case a stationary front bifurcates to a pair of fronts propagating in opposite directions, i.e., with positive and negative velocities. For the sake of definiteness, we shall consider front solutions traveling from $u = v = 1/2$ when $\xi \to -\infty$ to $u = v = 0$ when $\xi \to +\infty$. In this case the velocity of fronts is positive and the wave profiles read[1]

$$\begin{aligned} u_1(\xi) &= A_{11}\mathrm{e}^{\lambda_1\xi} + A_{12}\mathrm{e}^{\lambda_2\xi} + 1/2, \\ u_2(\xi) &= A_{21}\mathrm{e}^{\lambda_1\xi} + A_{22}\mathrm{e}^{\lambda_2\xi} + A_{23}\mathrm{e}^{\lambda_3\xi} + A_{24}\mathrm{e}^{\lambda_4\xi}, \\ u_3(\xi) &= A_0\mathrm{e}^{-c\xi}, \\ v_1(\xi) &= B_{11}\mathrm{e}^{\lambda_1\xi} + B_{12}\mathrm{e}^{\lambda_2\xi} + 1/2, \\ v_2(\xi) &= B_{21}\mathrm{e}^{\lambda_1\xi} + B_{22}\mathrm{e}^{\lambda_2\xi} + B_{23}\mathrm{e}^{\lambda_3\xi} + B_{24}\mathrm{e}^{\lambda_4\xi}, \\ v_3(\xi) &= B_0\mathrm{e}^{-c\xi}, \end{aligned} \tag{2}$$

where

$$\begin{aligned} \lambda_{1,2} &= -c/2 + \sqrt{c^2/4 + (\eta+1)/2 \pm \sqrt{(\eta+1)^2/4 - 2\eta}}, \\ \lambda_{3,4} &= -c/2 - \sqrt{c^2/4 + (\eta+1)/2 \pm \sqrt{(\eta+1)^2/4 - 2\eta}} \end{aligned} \tag{3}$$

and

$$\begin{aligned} B_{m1,3} &= [(\eta-1)/2 + \sqrt{(\eta-1)^2/4 - \eta}]A_{m1,3}, \\ B_{m2,4} &= [(\eta-1)/2 - \sqrt{(\eta-1)^2/4 - \eta}] \\ &\quad \times A_{m2,4},\ m = 1, 2. \end{aligned} \tag{4}$$

Thus, the first terms u_1, v_1 contain exponentials growing with increasing ξ, whereas the third terms u_3, v_3 contain exponentials decaying with growing ξ at positive velocities. All three terms for u and v are patched together using matching conditions for functions and their derivatives:

– patching at the first point $u(\xi = \xi_0) = a$:

$$\begin{aligned} &\sum_{n=1}^{2} A_{1n}e^{\lambda_n\xi_0} + 1/2 = \sum_{n=1}^{4} A_{2n}e^{\lambda_n\xi_0}, \\ &\sum_{n=1}^{2} A_{1n}\lambda_n e^{\lambda_n\xi_0} = \sum_{n=1}^{4} A_{2n}\lambda_n e^{\lambda_n\xi_0}, \\ &\sum_{n=1}^{2} A_{1n}e^{\lambda_n\xi_0} + 1/2 = a, \\ &\sum_{n=1}^{2} B_{1n}e^{\lambda_n\xi_0} + 1/2 = \sum_{n=1}^{4} B_{2n}e^{\lambda_n\xi_0}, \\ &\sum_{n=1}^{2} B_{1n}\lambda_n e^{\lambda_n\xi_0} = \sum_{n=1}^{4} B_{2n}\lambda_n e^{\lambda_n\xi_0}; \end{aligned} \tag{5a}$$

– patching at the second point $u(\xi = \xi_0^*) = \varepsilon$:

$$\begin{aligned} &\sum_{n=1}^{4} A_{2n}e^{\lambda_n\xi_0^*} = A_0 e^{-c\xi_0^*}, \\ &\sum_{n=1}^{4} A_{2n}\lambda_n e^{\lambda_n\xi_0^*} = -cA_0 e^{-c\xi_0^*}, \\ &A_0 e^{-c\xi_0^*} = \varepsilon, \\ &\sum_{n=1}^{4} B_{2n}e^{\lambda_n\xi_0^*} = B_0 e^{-c\xi_0^*}, \\ &\sum_{n=1}^{4} B_{2n}\lambda_n e^{\lambda_n\xi_0^*} = -cB_0 e^{-c\xi_0^*}. \end{aligned} \tag{5b}$$

We solve this system numerically (for $\xi_0 = 0$) and obtain the speed as a function of the model parameters ε and a for fixed η. [2] The graphical representations of the speed versus a and ε are illustrated in Figures 1 and 2. The first diagram (Fig. 1) displays front speed curves, c versus ε, for different values of a and $\eta = 0.1$. For each value of ε we have two possible front solutions with different speeds: the upper and lower branches correspond to fast and slow fronts respectively. One expects, as in the case of systems without cutoffs [14], that the faster front corresponds to a stable wave while the slower front corresponds to an unstable wave. There are two critical values, a_{crit} and $\varepsilon_{\mathrm{crit}}$, which are connected to each other. So, $\varepsilon_{\mathrm{crit}}$ appears when $a > a_{\mathrm{crit}}$ and a_{crit} is between 0.27 and 0.28 for $\eta = 0.1$. Fronts propagate with positive velocities for $\varepsilon > \varepsilon_{\mathrm{crit}}$, i.e., there appears a limited interval of ε where fronts with a positive speed do not exist. Figure 1 also shows that the curves for fronts with $a > a_{\mathrm{crit}}$ lie "inside" those fronts with $a < a_{\mathrm{crit}}$. Notice that for $a = 0.28$ the speed is not defined for all values of the cutoff threshold ε. Another interesting result is that the speed increases with ε for fast fronts, as occurs when a cutoff is imposed around the unstable state in a pushed front, and decreases with ε for a slow front, as occurs when a cutoff is imposed around the

[1] Ito and Ohta [13] obtained exact solutions for a motionless case and a propagating-pulse solution in the large inhibitor diffusion coefficient approximation. We consider here the system with equal diffusion constants. In this situation all solutions are exact.

[2] This parameter is fixed thorough the paper.

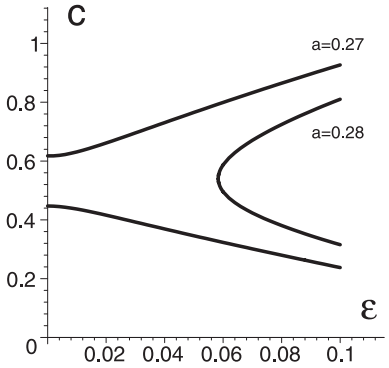

Fig. 1. Speed versus cutoff threshold for $\eta = 0.1$. The convergence of two front solutions. This is cutoff-dependent version of the nonequilibrium Ising-Bloch bifurcation [15].

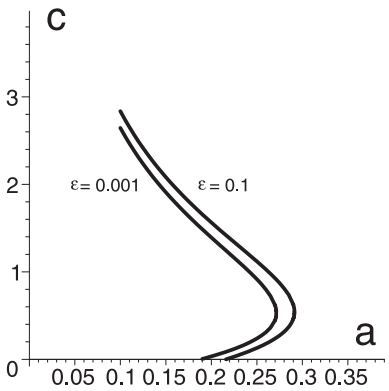

Fig. 2. Speed versus discontinuity position for $\eta = 0.1$. The shift of the front speed due to the cutoff is shown.

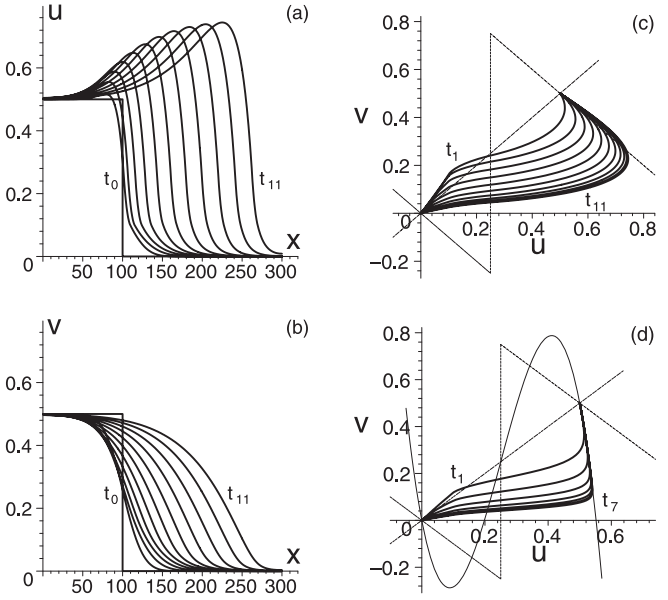

Fig. 3. Formation of a front from step initial condition. Spatial profiles (a) $u(x,t)$ versus x , (b) $v(x,t)$ versus x and (c) the $u-v$ diagram are shown for discrete t: $t_m = 2000m, 0 \le m \le 11$. The other parameters are fixed at $\varepsilon = \eta = 0.1$ and $a = 0.25$. For (a)–(c) we use the piecewise linear function $f(u,v) = -u - \theta(u-a) - v$ and for (d) we use the cubic nonlinearity $f(u,v) = 5u - 1 - (4u-1)^3 - v$. In the last case the $u-v$ diagram is shown for $t_m = 2000m, 0 \le m \le 7$. The dashed lines show null-clines, $f(u,v) = 0$ (piecewise linear) and $g(u,v) = 0$, the thin solid line displays the cubic nonlinear function, $f(u,v) = 0$.

unstable state in pulled fronts. At $\varepsilon = \varepsilon_{\rm crit}$, both branches join each other. The occurrence of such a convergence scenario can be explained by a nonequilibrium Ising-Bloch bifurcation [15] in the asymmetric case. A plot of the solutions, $c = c(\eta)$, in the (c, η) plane yields the saddle-node bifurcation diagram. The third branch of the bifurcation diagram occurs for negative speed values. We refer to the faster front as a Bloch front and to the slower front as an Ising front. This front bifurcation indicates where, in parameter space (ε, a), we should expect an initial pattern of domains decaying toward a uniform state and where it develops into a stable traveling wave. We will demonstrate below numerically this qualitative behavior.

In Figure 2 we plot front speed curves, c versus a, for different values of ε and $\eta = 0.1$. Each curve has a well defined knee. The knees indicate the existence of neutrally stable fronts out of which bifurcate the stable and unstable fronts [14]. We observe that the minimum value of c on each speed curve tends to zero for specific values of a depending on ε. Although it has not been displayed in Figure 2 the curves cross the horizontal axis toward negative values of the speed. In the opposite extreme, when $a \to 0$ the speed grows without limit.

We have also performed numerical calculations to determine further properties of fronts for equation (1). In all of the numerical results illustrated here we took $\varepsilon = \eta = 0.1$. For numerical integration, we employed a simple finite-difference scheme with $\Delta x = 0.1, 1 < x \le 300, \Delta t = 0.001$, and a zero-flux condition, $\partial u/\partial x = 0$ and $\partial v/\partial x = 0$, at both boundaries. To study how patterns are affected by the front bifurcation, we begin with a single step initial condition. The fronts emerging from step initial conditions are illustrated in Figures 3 and 4. Spatial profiles $u(x,t), v(x,t)$ and $u - v$ diagrams are shown for discrete t taking the maximum time to be $t_m = 2000m$. In Figure 3 we take $\varepsilon = \eta = 0.1$ and $a = 0.25$ while for Figure 4 we take $\varepsilon = \eta = 0.1$ and $a = 0.3$. It can be clearly seen from $u - v$ diagrams (Figs. 3c and 4c), that the $u - v$ curves asymptotically tend to uniformly translating solutions. Our numerical calculations demonstrate that if the parameters a, η or ε lie in a certain subset of values for which the analytical speed is not defined (see, for example, Figure 2 with $\varepsilon = \eta = 0.1$ and $a > 0.29$) then it is possible to find a front traveling with negative speed: Figure 3a shows a front moving to the right, i.e., propagating with positive velocity, whereas Figure 4a illustrates a front moving to the left (negative speed). The question we address here is how front solutions connecting the two states differ from those found for $\varepsilon = 0$. In the case without cutoff, if the system is prepared in the state 1/2 and perturbed locally on the left edge, then a front will propagate to the right, $c > 0$. On the other

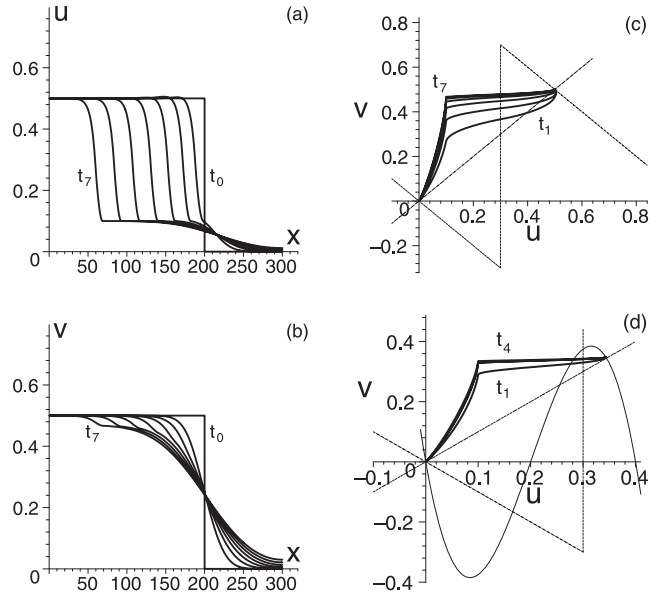

Fig. 4. Formation of a front from step initial condition. Spatial profiles (a) $u(x,t)$ versus x, (b) $v(x,t)$ versus x and (c) the $u-v$ diagram are shown for discrete t: $t_m = 2000m, 0 \leq m \leq 7$. The other parameters are fixed at $\varepsilon = \eta = 0.1$ and $a = 0.3$. For (a)–(c) we use the piecewise linear function $f(u,v) = -u - \theta(u-a) - v$ and for (d) we use the cubic nonlinearity $f(u,v) = 5u - 1 - (4u-1)^3 - v$. In the last case the $u-v$ diagram is shown for $t_m = 2000m, 0 \leq m \leq 4$. The dashed lines show null-clines, $f(u,v) = 0$ (piecewise linear) and $g(u,v) = 0$, the thin solid line displays the cubic nonlinear function, $f(u,v) = 0$.

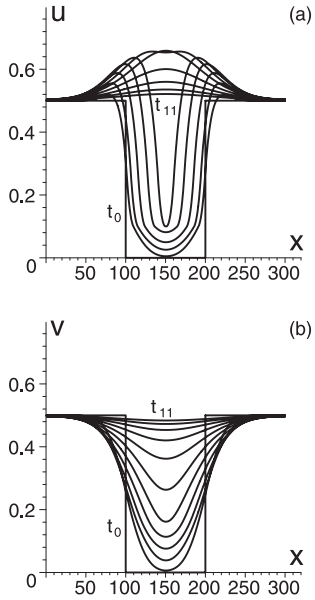

Fig. 5. Collision of two fronts. Spatial profiles (a) $u(x,t)$ versus x and (b) $v(x,t)$ versus x are shown for discrete t: $t_m = 2000m, 0 \leq m \leq 11$. The other parameters are fixed at $\varepsilon = \eta = 0.1$ and $a = 0.25$.

hand, preparing the system in the state 0 and perturbing it locally at the right edge of the domain, then the front propagates to the left, $c < 0$ [16]. In our preliminary calculations (not shown here) for $\varepsilon \neq 0$, we have prepared the system in a symmetrically perturbed state, $u(x,0) = v(x,0) = 0.5\theta(x - x_{\max}/2)$ and observed how fronts travel. We have found that emerging fronts propagate in opposite directions when the discontinuity parameter a changes from $a = 0.2$ to $a = 0.3$, which is in agreement with Figure 2. After that, we have perturbed the system at the edge lying in the opposite propagation direction as Figures 3 and 4 demonstrate.

Notice that the cutoff does not alter the qualitative form of the front with positive velocity, however, the front with negative speed returns slowly to the state at $u = v = 0$ in the cutoff region, so that the cutoff zone transforms the front profile (Figs. 4). Typical traveling wave solutions for the system (1) without cutoff, pass through the region in u with negative values. The same holds for the traveling pulse, or solitary wave, solutions for the excitable system. In this case the trailing edge of the pulse (the wave pulse back) also reaches negative values of u. In the system with cutoff considered here we see that both fronts (with positive and negative velocities) travel only in the region of the *positive* values of u, i.e., the effect of the cutoff is to shift the wave profiles to the positive value interval for both u and v.

Finally, we have briefly considered here another type of nonlinearity, the functions of the cubic type $f(u,v) \propto u - u^3 - v$, to provide some evidence of the generality of the phenomenon and to compare with the results obtained above for their piecewise linear approximations. Figures 3d and 4d show the $u-v$ diagrams for the symmetric ($a = 0.25$) and asymmetric ($a = 0.3$) cases, respectively. We see that the dynamical behaviors are in an agreement with those displayed in Figures 3c and 4c. The only difference is in t_n: the $u-v$ diagrams in Figures 3d and 4d are shown for $m = 0, 1, 2, ..., 7$ and $m = 0, 1, 2, ..., 4$, respectively, because at these times both fronts are completely formed. Thus, according to the above simulations, we strongly emphasize that the appearance of a front with negative velocity is not limited to the piecewise linear reaction-diffusion system in the form of equation (1) but it presents more general bistable kinetics.

For the same parameter values, however, there exist simultaneously the rightward and leftward moving fronts or, more precisely, the front and back. This situation can be realized under an appropriate choice of the initial conditions. In Figures 5 and 6 we take for initial data at $t = t_0$ two square steps. The other parameters are fixed at $\varepsilon = \eta = 0.1, a = 0.25$ and $a = 0.3$, as above in Figures 3 and 4, respectively. Then the numerical simulations show the dynamics of the collisions of the front and the back. When these two waves reach each other they annihilate and, in this case, the medium returns ultimately to the stable state ($u = v = 1/2$ in Figs. 5 and $u = v = 0$ in Figs. 6. Note that $u = v = 0$ and $u = v = 1/2$ are metastable states in Figs. 5 and 6 respectively due to the different value of a taken in each figures). The relaxation phenomena towards a stable state for $\varepsilon = 0$ is considered in reference [16], where a transition from transient to

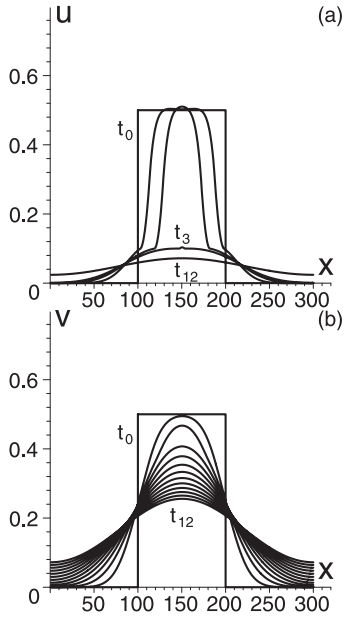

Fig. 6. Collision of two fronts. Spatial profiles (a) $u(x,t)$ versus x and (b) $v(x,t)$ versus x are shown for discrete t: $t_m = 2000m$, $m = 0, 1, 2, 3, 12$ (a) and $0 \le m \le 12$ (b). The other parameters are fixed at $\varepsilon = \eta = 0.1$ and $a = 0.3$.

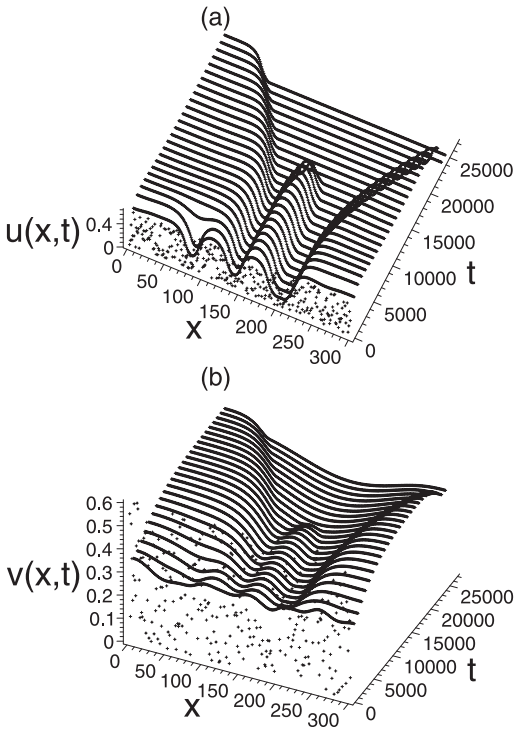

Fig. 7. 3D-diagrams: (a) $u(x,t)$ versus x and t (b) and $v(x,t)$ versus x and t starting from a random initial condition at $t_0 = 0$ on the interval $u, v \in [0, 0.6]$. The other parameters are fixed at $\varepsilon = 0.001, \eta = 0.1$ and $a = 0.25$.

persistent patterns is explored. The propagating domains do not necessarily annihilate in a head-on collision but can behave as if they are elastic objects. In this context, the dynamics are usually taken to be excitable and in this case there is only one stable singular point, the state $u = v = 0$. An adequate initial displacement from the stable leads to a large path before the return. This is a formation of an another type of traveling wave, a pulse. This significant change in the qualitative behavior of patterns can be attributed to two related factors; the appearance of front multiplicity due to the nonequilibrium Ising-Bloch bifurcation and the appearance of a second independent field.

Initial conditions play a critical role in the existence of traveling waves [1]. If the perturbation has a maximum u lower than the threshold $u = a$ then the kinetics cause u to return to the origin and the spatial perturbation simply dies out. On the other hand if the perturbation is larger than the threshold $u = a$ then the kinetics initiate a large domain in both u and v. The influence of initial disturbances on propagating fronts can be shown when a random initial condition is considered. Figure 7 shows a 3D-diagram for complex wave dynamics starting from random initial sets for $u(x,t)$ and $v(x,t)$ at $t_0 = 0$ on intervals for u and v from 0 to 0.6. One can see that the disturbed region forms different domains of the front, back and pulse-like shapes. As the disturbed region slowly returns to the stable state, the metastable state either shrinks or expands (the pulse-like wave collapses) and the front and back domains become widely separated from each other, so that at $t = 25\,000$ only a single front exists.

Conclusions

Using a combination of semi-analytical analysis and numerical simulation, we have shown that when the two-component piecewise linear bistable reaction-diffusion system is solved on a finite domain subject to zero flux boundary conditions, uniformly traveling waves with different speeds develop. We have shown the formation of traveling fronts from step initial conditions, the collision of fronts from two-step initial conditions and the existence of other types of waves under random initial conditions. The numerical study demonstrates that there are fronts propagating with negative velocity if $\varepsilon < \varepsilon_{\rm crit}$ constituting the cutoff-version of the nonequilibrium Ising-Bloch bifurcation. The speed of the Bloch front increases with ε while the speed of the Ising front decreases with ε.

E.P.Z. thanks Prof. J. Casas-Vázquez and his group for warm hospitality in Barcelona, V.M. acknowledges the project BFM2003-06033.

References

1. J.D. Murray, *Mathematical Biology* (Springer-Verlag, third edition, 2003)
2. L.S. Tsimring, H. Levine, D.A. Kessler, Phys. Rev. Lett. **76**, 4440 (1996)

3. E. Brunet, B. Derrida, Phys. Rev. E **56**, 2597 (1997)
4. D.A. Kessler, Z. Ner, L.M. Sander, Phys. Rev. E **58**, 107 (1998)
5. D. Panja, W. van Saarloos, Phys. Rev. E **66**, 015206(R) (2002)
6. *Chemical Waves and Patterns*, edited by R. Kapral, K. Showalter (Kluwer, Dordrecht, 1995)
7. D.A. Kessler, H. Levine, Nature **394**, 556 (1998)
8. I. Golding, Y. Kozlovsky, I. Cohen, E. Ben-Jacob, Physica A **260**, 510 (1998)
9. V.S. Zykov, *Simulation of Wave Processes in Excitable Media* (Manchester University Press, New York, 1987)
10. J. Rinzel, J.B. Keller, Biophys. J. **13**, 1313 (1973)
11. J.P. Keener, J.J. Tyson, Physica D **21**, 307 (1986)
12. A. Hagberg, E. Meron, Chaos **4**, 477 (1994)
13. A. Ito, T. Ohta, Phys. Rev. A **45**, 8374 (1992)
14. J. Rinzel, D. Terman, SIAM J. Appl. Math. **42**, 1111 (1982)
15. P. Coullet, J. Lega, B. Houchmanzadeh, J. Lajzerowicz, Phys. Rev. Lett. **65**, 1352 (1990); A. Hagberg, E. Meron, Phys. Rev. E **48**, 705 (1993)
16. A. Hagberg, E. Meron, Nonlinearity **7**, 805 (1994)
17. P. Muruganandam, M. Lakshmanan, Chaos **7**, 476 (1997)